Appl. Phys. B 74, 765–775 (2002)
DOI: 10.1007/s00340-002-0922-8

Applied Physics B
Lasers and Optics

E.D. MISHINA[1,2,✉]
A.I. MOROSOV[1]
Q.-K. YU[2]
S. NAKABAYASHI[2]
T. RASING[3]

Nonlinear optics for surface phase transitions

[1] Moscow Institute of Radioengineering, Electronics and Automation, prosp. Vernadskogo 78, 117454 Moscow, Russia
[2] Department of Chemistry, Faculty of Science, Saitama University, 255, Saitama, 338-8570, Japan
[3] Research Institute for Materials, University of Nijmegen, Toernooiveld 1, 6525 ED Nijmegen, The Netherlands

Received: 15 January 2002
Published online: 11 June 2002 •

ABSTRACT A general approach of second-harmonic generation (SHG) studies for surface phase transitions (PTs) is presented, with a thermodynamic classification of surface PTs and their relation to SHG parameters. The symmetry aspects of SHG near a surface PT are discussed, including issues connected with separation of surface and bulk contributions and the role of atomic and mesoscopic inhomogeneities. This approach is illustrated by applying it to two systems revealing a (near-) surface PT: single-crystalline $SrTiO_3$ near a bulk structural PT and single-crystalline Au in an electrochemical cell revealing an order–disorder and a reconstructive PT.

PACS 42.65.ky; 68.35.Rh

1 Introduction

Optical second-harmonic generation (SHG) with its high surface and symmetry sensitivity has been proven to be a powerful tool for studying surface phase transitions (PTs). Already, the first experiments on surface phase transitions (time-resolved laser-induced silicon melting [1], $(1 \times 1) \rightarrow (7 \times 7)$ surface reconstruction of Si(111) [2]), showed the power of the SHG technique for such kinds of studies. During the last two decades the number of surface PTs that were studied using SHG has continuously increased. Despite the development in recent years of more direct experimental techniques like scanning tunnelling microscopy (STM) [3], low-energy electron diffraction (LEED) [4], and most recently synchrotron X-ray diffraction (XRD) [5], there are still many conditions for which SHG remains the best choice for studying surface PTs. First of all these are PTs at buried interfaces, when for example the surface undergoing a PT is in contact with a liquid or a PT in a near-surface layer with a thickness of several lattice constants, which can be considered as a solid–solid interface. Another class of examples is studies of the dynamics of surface PTs. And where the buried interfaces can sometimes also be studied (with some limitation) using other techniques, (nonlinear) optical techniques do not have any rivals in studying dynamics, as using state-of the art lasers time scales from hours down to femtoseconds can be exploited.

In this paper we discuss a general approach of SHG studies of surface phase transitions. We give a symmetry analysis of SHG radiation during a surface PT, in which contributions from surface and bulk are discussed, as well as the role of atomic and mesoscopic scale inhomogeneities in connection with fluctuations or with a mixture of phases. After that a thermodynamic classification of surface PTs and their relation to SHG parameters is given. This approach is applied to two systems revealing a (near-)surface PT: single-crystalline $SrTiO_3$ (STO) with a structural PT and a single-crystalline Au(111) electrode undergoing different types of surface PT depending on electrochemical conditions. For each observed PT, at the end of the appropriate section the main results that can be obtained from SHG studies are emphasised.

2 Theoretical consideration

There are several ways to classify surface phase transitions: according to the change of symmetry (order–disorder, order–order, incommensurate), according to the behaviour of thermodynamic functions (first order, second order), according to the localisation of the PT layer (subsurface, near-surface, in adsorbate layer), or according to their nature (structural, magnetic, ferroelectric). As far as SHG is concerned, the symmetry of the surface plays the most important role in distinguishing different phases. Therefore we will first of all classify the surface PTs according to symmetry. Apart from symmetry, in most cases the surface band structure changes. This requires an analysis of the spectrum of the surface states and its changes during the PT. Examples of this can be found in the literature [15–21] and will not be further discussed here. Finally, a thermodynamic classification will be given with regard to the SHG parameters. In the following general consideration we will use the term 'surface PT' without specifying its localisation, which will be done in the examples.

It is important to note that when a surface is studied by SHG the light/media interaction depth is very small. In order to distinguish between bulk and surface, the interplay between the symmetry and depth of the nonlinear polarisation source is exploited: for centrosymmetric media the thin surface layer with a high dipole-type nonlinear optical polarisation gives

✉ E-mail: elena@chem.saitama-u.ac.jp

a SHG field strength comparable to the effective bulk-layer contribution, with a much weaker quadrupole-type nonlinear polarisation. It means that when using SHG mostly PTs at the surface of centrosymmetric bulk media can be studied. Hence only interfaces of centrosymmetric media will be considered in the following.

2.1 *Symmetry analysis of surface PTs*

The nonlinear polarisation of the surface is of dipole type and is determined by its point-group symmetry through the nonlinear susceptibility tensor $\hat{\chi}^{(\mathrm{D})}$:

$$P_i^{\mathrm{D}}(2\omega) = \chi_{ijk}^{(\mathrm{D})} E_j(\omega) E_k(\omega), \tag{1}$$

where $\boldsymbol{E}(\omega)$ is the electric field of the incident wave. The structure of $\hat{\chi}^{(\mathrm{D})}$ (nonzero tensor components) for any type of surface symmetry can be found in [6]. This surface polarisation interferes with the quadrupole-type polarisation of the bulk, which for dielectrics is described by

$$P_i^{\mathrm{Q}}(2\omega) = \chi_{ijkl}^{(\mathrm{Q})} E_j(\omega) \nabla_k E_l(\omega), \tag{2}$$

where $\chi_{ijkl}^{(\mathrm{Q})}$is the bulk nonlinear susceptibility tensor. In (2) the nonlinear source arises from electrons that are localised on the atom core. In the case of a delocalised electron system (semiconductors, metals) and simple cubic symmetry, the nonlinear polarisation can be written as [7]

$$P_i^{\mathrm{Q}} = \gamma \nabla_i (E \cdot E) + \zeta E_i \nabla_i E, \tag{3}$$

where γ and ζ are constants.

The nonlinear susceptibility tensor components or at least their linear combination can be obtained by measuring the SHG intensity (for various combinations of input and output polarisation) during rotation of the sample around its normal. In (1) and (2), depending on the surface symmetry, both isotropic (independent of surface orientation) and anisotropic (dependent on surface orientation) components can be present. In (3) the first term corresponds to the isotropic contribution, and the second term is anisotropic. The source of nonlinear polarisation described by the second term of (3) is localised in the bulk of the crystal. The first term is more complicated. It can be expressed in terms of phenomenological complex parameters a, b, and d, introduced by Rudnick and Stern [8]. The parameters a and b determine the excitation efficiency of the normal and tangential components of the surface current, and therefore the corresponding polarisation is localised in the near-surface region. The parameter d is of pure bulk origin. It was shown in [9] that the surface parameter a gives the main contribution to the SHG field, and that b and d can be neglected. So, finally, from (3) we obtain isotropic surface and anisotropic bulk contributions.

A symmetry analysis of the SHG intensity gives information on a surface PT if the surface symmetry changes while the bulk symmetry remains the same. If there is no interaction between bulk and surface (the case of a near-surface PT), the polarisation described by (1) and (2) can be summed up independently into a total SHG polarisation. If a PT occurs in the topmost or adsorbed (sub)monoatomic layer, electrons in two neighbouring layers are not independent and the whole 'sandwich' should be considered on top of the bulk, which in turn can be taken into account independently. So we have to construct an effective $\hat{\chi}^{(\mathrm{D})}$for the surface 'sandwich' and then sum up (1) with (2) or (3).

2.1.1 SHG field at ordered surfaces; order–order phase transitions.

If a crystal is imagined to be cut into two pieces with all atoms and bonds kept in their bulk positions an imaginary (1×1) surface appears. For such a surface there is no way to distinguish between the surface and bulk contributions and therefore the surface symmetry analysis becomes useless. A real surface is different: after the crystal is cleaved the surface usually undergoes a relaxation process leading to the appearance of different kinds of surface states and surface reconstructions. If the surface undergoes a phase transition, both the energy of the surface states and the symmetry can be changed. Therefore the surface phase transitions can be probed either by SHG spectroscopy or by the analysis of the SHG symmetry properties. In this paper we focus on the symmetry analysis.

For any type of surface symmetry the SH field generated at a single-crystalline (nonreconstructed) surface can be expressed as

$$E_{\mathrm{Nrec}} = f_0 + \sum_{i=1}^{3} \left(c_i \cos i\Psi + s_i \sin i\Psi\right), \tag{4}$$

where Ψ is the azimuthal angle of the crystal relative to one of the crystallographic axes; f_0, c_i, and s_i are linear combinations of $\hat{\chi}^{(\mathrm{D})}$ and $\hat{\chi}^{(\mathrm{Q})}$ tensor components (or $\hat{\chi}^{(\mathrm{D})}$, γ, and ζ) depending on the studied system.

For low-index surfaces (4) becomes simple. For example, for a (100) surface of a cubic crystal with symmetry ($m3m$), E_{Nrec} is constant for a SH wave polarised in the plane of incidence (p-out) and equals zero for a SH wave polarised perpendicular to the plane of incidence (s-out). For a (110) surface of the same crystal $E_{\mathrm{Nrec}} = a_0 + a_2 \cos(2\Psi)$ for p-out (zero for s-out). For a (111) surface

$$E_{\mathrm{Nrec}} = f_0 + c_3 \cos(3\Psi) \tag{5}$$

for p-out and

$$E_{\mathrm{Nrec}} = s_3 \sin(3\Psi) \tag{6}$$

for s-out.

If a surface reconstruction takes place, two possibilities arise.

1) The symmetry of the surface layer is not changed. This happens for instance at a hexagonal surface for the $1 \times 1 \rightarrow \sqrt{3} \times \sqrt{3}$ and $\sqrt{3} \times \sqrt{3} \rightarrow 2\sqrt{3} \times \sqrt{3}$ reconstructions or for a rectangular surface for the $(1 \times 1) \rightarrow (2 \times 2)$ reconstruction. In this case the expressions for the nonlinear polarisation are not changed, and the impact of the reconstruction on the SHG response only appears as a change of (existing) Fourier components in (4). The origin of this change depends strongly on the nature of the studied surface and will be discussed together with the examples.

2) The symmetry of the surface is changed. This happens for instance for more complicated reconstructions like $(1 \times 1) \rightarrow (23 \times \sqrt{3})$ (and all other types with a high ratio of reconstructed/nonreconstructed surface lattice constants). The most general result of such a reconstruction is that the high-order symmetry in the topmost layer is replaced by a lower-order symmetry. Considered together with the underlying layer the total symmetry is lowered as well. This means that additional terms appear in the expression for the nonlinear polarisation together with possible changes of the previously existing terms. The situation gets more complicated by domain formation that generally accompanies such a reconstruction process. A comprehensive analysis of the influence of $23 \times \sqrt{3}$ domain formation at a hexagonal (111) surface on the SHG anisotropy is given in [10]. It results in the appearance of one-fold and two-fold components in (5) and (6) with the azimuthal angles shifted by Ψ_1 and Ψ_2 from the position of the three-fold components:

$$E_{\text{rec}} = f_0 + c_1 \cos(\Psi - \Psi_1) + c_2 \cos\left(2(\Psi - \Psi_1)\right) + c_3 \cos(3\Psi), \tag{7}$$

where c_1 andc_2 as well as Ψ_1 and Ψ_2 depend on the domain spatial distribution (density of uncompensated domains). It is important to note that the presence of uncompensated domains changes the azimuthal dependence of the SHG field only if the symmetry of individual domains is different from the symmetry of the nonreconstructed surface. If not, than the presence of domains changes only the magnitude of existing components.

2.1.2 SHG in an incommensurate surface (layer); commensurate–incommensurate PTs.

An incommensurate structure can appear for a PT driven by the adsorption of ions. The topmost layer of adsorbates can be perfectly ordered with a well-defined symmetry. However, if this surface layer or adsorbates develops a nonrational periodicity with respect to the bulk, the total top 'sandwich' structure is incommensurate. With respect to symmetry, an incommensurate structure corresponds to a random or isotropic structure that gives only an isotropic contribution to the p-out SHG field (with zero s-in, s-out). Therefore a PT from ordered to incommensurate structure will result in an increase of the isotropic component of the surface susceptibility. (The change in anisotropic components during a commensurate/incommensurate PT calls for different explanations: see Sect. 2.2.)

2.1.3 SHG at a disordered surface; order–disorder PTs.

Two kinds of disordering of the surface layer are possible during a PT: atomic random and island(nucleus)-random. Both of them should be considered as atomically rough but with a different in-plane correlation length. An atomically rough surface was studied in [11, 12] for a silicon/silicon oxide interface. It was shown that atomic roughness leads to a change of the isotropic component in the SHG field. The most distinguishable result can be obtained for polarisation combinations for which the isotropic component in the case of a flat surface is forbidden (s-in, s-out). Therefore an order–disorder PT with random atomic scale inhomogeneities should result in the appearance of a (forbidden for s-in, s-out) isotropic contribution in the nonlinear polarisation.

In-plane inhomogeneities of the surface with a correlation length that is of the same order of magnitude as the wavelength were studied in [13, 14]. It was shown that such inhomogeneities give rise to an incoherent background and the scattering indicatrices (dependences of SHG intensity on scattering angle) give a measure of the correlation length. Therefore an order–disorder PT with mesoscopic inhomogeneities should result in the appearance of scattered background.

2.2 *Thermodynamic classification of surface PTs*

Phase transitions can be classified according to the behaviour of the free energy F, which in classic phase-transition theory is a function of temperature and pressure: $F(p, T)$ [4]. For surface PTs the free energy can also be a function of coverage and electric field. When the first derivatives of the free energy $(\partial F/\partial T)_p$ or $(\partial F/\partial p)_T$ change discontinuously the transition is called first order. When only the second-order derivative changes discontinuously (with the first-order derivative being continuous) a PT is called second order.

For first-order PTs not only the free energy, but also other equilibrium parameters (for example coverage, magnetisation), change discontinuously. Due to the presence of metastable states, co-existence of phases and hysteresis are observed instead of steps in the system parameters. Therefore the presence of hysteresis in the SHG field can be considered as evidence of a first-order PT.

In case of a second-order PT, the symmetry is lowered to one of the subgroups of the original point group and an order parameter η changes continuously. The free energy can then be expanded in a series of the order parameter (Landau–Ginzburg theory). The case of a three-component surface order parameter for a PT driven by a temperature change was discussed in [22]. Here we introduce an analogous expansion for a 2-D system and a one-component order parameter for a PT driven by an electric field normal to the metal surface:

$$F(\eta) = \frac{1}{2}A\eta^2 + \frac{1}{4}B\eta^4 + \frac{1}{2}C(\nabla\eta)^2. \tag{8}$$

Here, the coefficients A, B, and C are generally functions of temperature T, pressure p, electric field E, and coverage θ. For fixed T, p, and θ the first coefficient $A(E)$ becomes zero at the phase-transition point: $A(E_0) = 0$. Near E_0 one can obtain from (8)

$$F(\eta) = \frac{1}{2}A'\varepsilon\eta^2 + \frac{1}{4}B\eta^4 + \frac{1}{2}C(\nabla\eta)^2, \tag{9}$$

where $A\prime$ is constant and $\varepsilon = (E - E_0)/E_0$. As (9) coincides with the common Landau expansion for $\tau = (T - T_c)/T_c$ (with τ being substituted by ε), calculations of critical exponents are identical. Therefore the values of the critical exponent are equal as well:

$$\eta \propto \varepsilon^{\beta}. \tag{10}$$

The value of the critical exponent depends on the model: the mean-field approximation gives $\beta = 1/2$, the exact value for

the two-dimensional Ising model is $\beta = 1/8$, for the three-state Potts model $\beta = 1/9$ or $\beta = 1/12$ (depending on the site occupation) [23]. In the close vicinity of a second-order PT, fluctuations of the order parameter increase (critical behaviour), and this region can be described by scaling theory. According to the scaling hypothesis the nature and fine structure of the system do not play any role but only the dimension of the system (in our case 2-D), the symmetry of the order parameter, and the character of the interactions are important.

An additional way to distinguish between first- and second-order PTs is to study the dynamics of the process. In particular, in electrochemical systems this is based on the current transient while a step voltage is applied to the surface. For a first-order PT (nucleation and growth), it is given by [24]

$$j(t) = \kappa_2 t \mathrm{e}^{-(t/t_0)^2}. \tag{11}$$

For a second-order PT (random nucleation), it is given by [25]

$$j(t) = \kappa_1 \mathrm{e}^{-t/t_0}. \tag{12}$$

In these expressions κ_1 and κ_2 are amplitudes and t_0 is a time constant.

2.2.1 SHG parameters for first- and second-order surface PTs.

There is no general model to describe the nonlinear susceptibility during a surface PT. The first attempt has been made in [22]. For a second-order PT (not magnetic and not properly ferroelastic [26]) the surface nonlinear susceptibility can be expressed in terms of the surface order parameter η_0 as

$$\chi^{\mathrm{L}}_{ijk} = \chi^{\mathrm{H}}_{ijk} + \vartheta_{ijklm}\eta_{0l}\eta_{0m}, \tag{13}$$

where $\hat{\chi}^{\mathrm{L}}$ and $\hat{\chi}^{\mathrm{H}}$ are the nonlinear susceptibility tensor in the low- and high-symmetry phases respectively and $\bar{\vartheta}$ is a fifth-order tensor corresponding to the surface point-group symmetry. If the order parameter is one-component (scalar), (13) also can be used with $\bar{\vartheta}$ being a third-order tensor corresponding to the symmetry of the surface. The dependence of the order parameter on the PT-inducing external parameters (T, E) is described by (10).

For a first-order PT the concept of an order parameter cannot be used. In this case, theoretically, the SHG field should be a step function in a PT point. In reality the step is smoothed and hysteresis in the SH field is observed. Hence one can write for the effective nonlinear susceptibility for the range of external parameters where two phases co-exist:

$$\chi^{\mathrm{eff}}_{ijk}(T, E) = H(T, E)\chi^{\mathrm{H}}_{ijk} + L(T, E)\chi^{\mathrm{L}}_{ijk}, \tag{14}$$

where $H(T, E)$ and $L(T, E)$ are partial densities of the high-symmetry and low-symmetry phases respectively. This expression allows us to determine the partial densities of the two phases in the vicinity of a PT.

In the special case of a metal surface in an electrochemical environment, the SHG transient can be used to distinguish between first- and second-order PTs. For metals within a jellium model the isotropic term f_0 depends on the surface charge σ [27],

$$f_0(\sigma) \propto \alpha_0 + \alpha_1\sigma, \tag{15}$$

where α_0 and α_1 are constants. The charge transient can be calculated from (11) and (12), which give together with (15) the SHG transient:

$$f_0(\sigma) \propto \mathrm{e}^{-(t/t_0)^2} \tag{16}$$

for a first-order PT and

$$f_0(\sigma) \propto \mathrm{e}^{-t/t_0} \tag{17}$$

for a second-order PT.

3 Experiment

For studying a near-surface PT, single-crystalline $SrTiO_3$ (110) was used. Details of the structure and growth procedure are described in [22]. The crystal undergoes a bulk structural phase transition at $T_c = 105$ K; the near-surface PT was observed at $T^* = 150$ K.

A real surface PT was studied on single-crystalline Au (111); details of the preparation procedure are described in [28]. Cyclic voltammograms (current–voltage dependences) in 0.05 M sulfuric acid were measured after electrode preparation as evidence of the high quality of the surface [29]. In order to obtain different kinds of surface phase transitions, different electrolytes were used: 0.5 M sulfuric acid H_2SO_4 (see Sect. 4.2), 0.1 M sulfamate acid H_2NSO_3NH, 0.1 M sulfuric acid H_2SO_4 (see Sect. 4.3), and 1 mM $CuSO_4$ in 0.05 M H_2SO_4 (see Sect. 4.4). In all experiments the electrode voltage was measured relative to an saturated calomel electrode (SCE).

For the SHG experiments both femtosecond Ti:sapphire and nanosecond Nd:YAG laser systems were used. The Ti:sapphire laser (≈ 800 nm) had a pulse width of about 100 fs, a repetition rate of 78 MHz, and was focused onto a spot of 0.1 mm in diameter. For detection a photon-counting system was used. To measure the scattered background we either rotate the detection system (in the case of STO around the vertical axes to measure scattering indicatrices) or use a two-channel detection system, with one channel measuring the specular and the second channel the scattered signal. In this case the second photomultiplier tube (PMT) was located at the scattering angle of 20 degrees.

The YAG laser based system operates at a fundamental wavelength of 1064 nm, a pulse width of about 3.5 ns, and an energy per pulse of 3 mJ, and was focused onto a spot of about 0.5 mm in diameter. For detection a PMT (Hamamatsu H5784-06 photonic sensor with built-in amplifier) followed by a boxcar averager–integrator (Stanford Research SR245) for signal processing was used. For dynamic measurements, periodic (10–20 Hz) square pulses from a function generator triggered by the laser power supply were applied to the electrode. The delay time of the laser pulse with respect to the voltage pulse was varied in the range of 0–100 ms. In this way the SHG signal from the electrode was measured in different temporal states of a deposition/dissolution process. Details of dynamics measurements are presented in [28].

For both systems the polarisation of the fundamental wave was controlled by a Berek compensator, and of the SH waves by a Glan prism. The angle of incidence was kept at 45 degrees for STO and 30 degrees for the electrochemical measurements. The azimuthal anisotropy $I_{2\omega}(\Psi)$ was measured by rotating the sample around its normal. The SHG signal was discriminated spectroscopically by appropriate colour and bandpass filters.

4 Results and discussion

4.1 *Structural phase transition in a near-surface layer*

A structural PT in the subsurface layer was observed for the first time in single-crystalline $SrTiO_3$, which reveals a bulk structural PT from $m3m$ to $4/mmm$ point-group symmetry [22]. The near-surface PT was found at the temperature $T^* = 150$ K, which is 45 degrees higher than the bulk T_c. Here we want to show that these results fall under the general considerations of second-order phase transitions, namely the correlation of the SHG field with the order parameter. Additionally, we show the role of scattered radiation in these measurements.

As is shown in Sect. 2.3, for second-order PTs fluctuations of the order parameter increase in the vicinity of a PT, giving rise to intensive scattering of SHG radiation [30]. Figure 1a shows typical SHG scattering indicatrices for different temperatures. These measurements allow us to separate specular and scattered radiation: as the scattering profile is rather wide, we subtract the signal at the polar angle of 5 degrees from the total signal at zero polar angle; the difference is attributed to the specular signal. As can be seen in the temperature dependence of the scattered light (Fig. 1b), contrary to our expectation no scattering was found that could be attributed to surface critical phenomena. The smoothly increasing scattered intensity down to low temperatures must be attributed to critical phenomena connected with the low-temperature (40 K) incipient PT. As similar dependences are observed in transmission as well, we can conclude that this scattered radiation is generated in the bulk of the crystal. This is not surprising, because the scattered radiation is incoherent and the difference between transmission and reflection geometry based on the coherence length [22] disappears.

The temperature dependence of the pure coherent SHG field in the specular direction is shown in Fig. 2. Polarisation combinations are *s*-in, *p*-out and *p*-in, *p*-out. Above $T = 150$ K the coherent SHG equals zero within the error bar. In the temperature range $T < 150$ K these dependences are linear, with a change in slope at the bulk transition temperature $T_c = 105$ K. The temperature $T^* = 150$ K is attributed to a near-surface structural PT, and according to (10) and (13) these linear dependences indicate that the nonlinear susceptibility follows a general power law with the critical exponent $\beta = 1/2$ (mean-field approximation).

So, in summary, for the single-crystalline $SrTiO_3$ we find from our SHG data:

- a near-surface PT on the (110) surface at 150 K, i.e. 45 K above T_c of the bulk;
- the SHG field obeys a power-law dependence with the critical exponent $\beta = 1/2$;
- the scattered intensity due to fluctuations of the bulk order parameter is high, but no critical scattering from the surface was found.

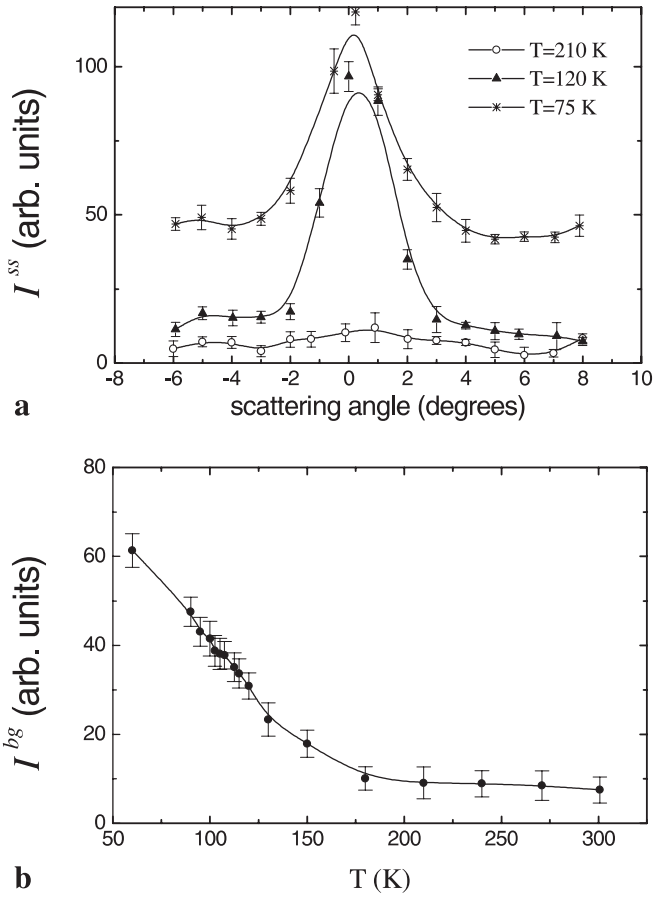

FIGURE 1 Observation of near-surface phase transition at $SrTiO_3$ (110): **a** scattering indicatrices of SHG intensity in reflection geometry for different temperatures; for exact specular direction the SHG signal is a superposition of two contributions: coherent (near-surface) and incoherent (bulk); **b** temperature dependence of SHG scattered intensity measured at the scattering angle of 6°

4.2 *Phase transitions in the surface layer*

4.2.1 Second-order order–disorder PT at an Au (111) surface induced by adsorption of sulfate anions.

There are two PTs at Au (111) in sulfuric acid: when the surface is negatively charged, the surface is $23 \times \sqrt{3}$ reconstructed; when the surface is positively charged, the surface is $\sqrt{3} \times \sqrt{7}$ reconstructed. There is some voltage range in between where the surface is nonreconstructed. The (1×1) to $(23 \times \sqrt{3})$ PT will be discussed elsewhere [31]. Here we focus on the order $(\sqrt{3} \times \sqrt{7}) \rightarrow$ disorder PT occurring at 0.8 V. Although this phase transition was widely studied by different LEED [33], in situ STM [32, 34], electrochemical [35], and SHG [10] experiments a thermodynamic classification (first or second order) of this PT is absent.

In the current–voltage dependence (cyclic voltammogram or CV) the PT manifests itself in a reversible way by narrow spikes at $U_0 = 0.78$ V. In STM measurements a $(\sqrt{3} \times \sqrt{7})$ surface reconstruction was observed [34] for $U > U_0$

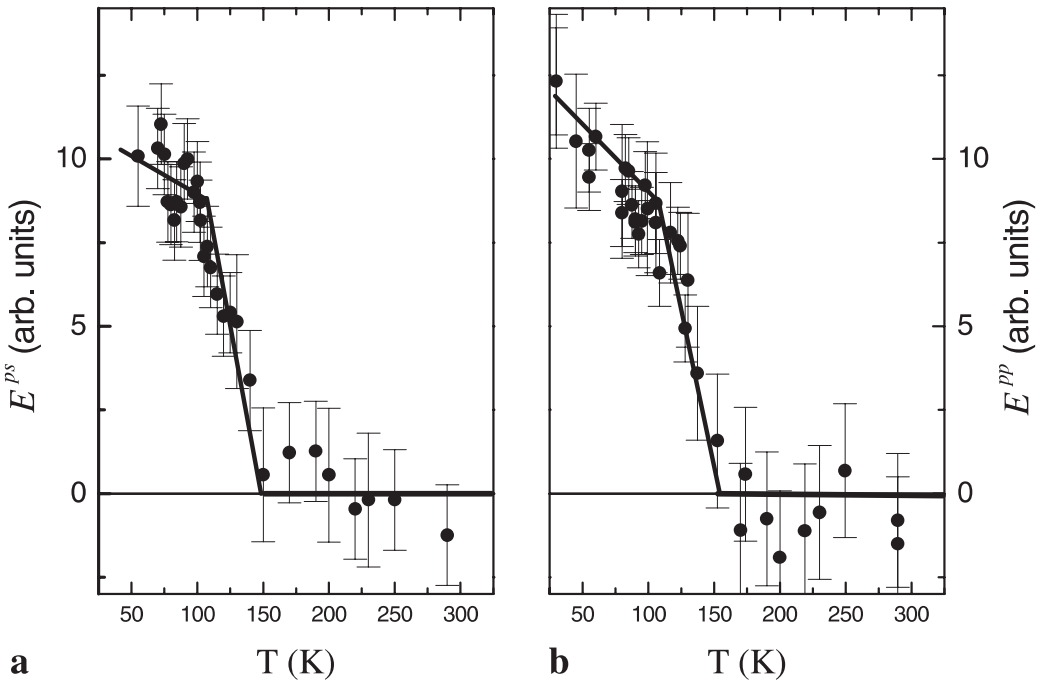

FIGURE 2 Observation of near-surface phase transition at $SrTiO_3$ (110): temperature dependence of coherent SHG field measured as the difference between the SHG intensities for 0° and 5° scattering angles. Polarisation combinations are *p*-in, *s*-out (**a**) and *p*-in, *p*-out (**b**). Fundamental wavelength is 760 nm

that is formed by sulfate anions. Sulfate anions start to adsorb randomly around 0.3 V, and the surface coverage increases (see Fig. 3a, thick line, data are taken from [35]). At U_0 it reaches the critical value of 0.2 and the order–disorder PT takes place (see Fig. 3, thin line). For $U > U_0$ the whole sample is divided into domains. Three types of domains exist with the point-group symmetry of each domain being m.

The azimuthal rotational dependences of SHG intensity at different electrode potentials are shown in Fig. 3b. In the ordered phase these dependences should be described by (7) with an appearance of one- and two-fold Fourier components at U_0. However the one-fold component is rather high for all potentials, and its change at U_0 does not exceed 5% (error bar for this type of measurements), while the change in the three-fold component is about 10%. This allows us to use (5) for the fitting procedure both for the nonreconstructed and reconstructed phases.

Further measurements have been done by measuring the SHG response simultaneously with the CVs. The SHG intensity was measured at the maximum ($\Psi = 0$), minimum ($\Psi = \pi/3$), and the intermediate points ($\Psi = \pi/6$) of the azimuthal dependence. The voltage dependence of the SHG intensity at the maximum (Fig. 3a, dots, *p*-in, *p*-out polarisation combination) reveals a break exactly at U_0. This break remains in the three-fold component, but does not exist in the isotropic component. No hysteresis in the voltage dependence of the SHG intensity is observed. The voltage dependence

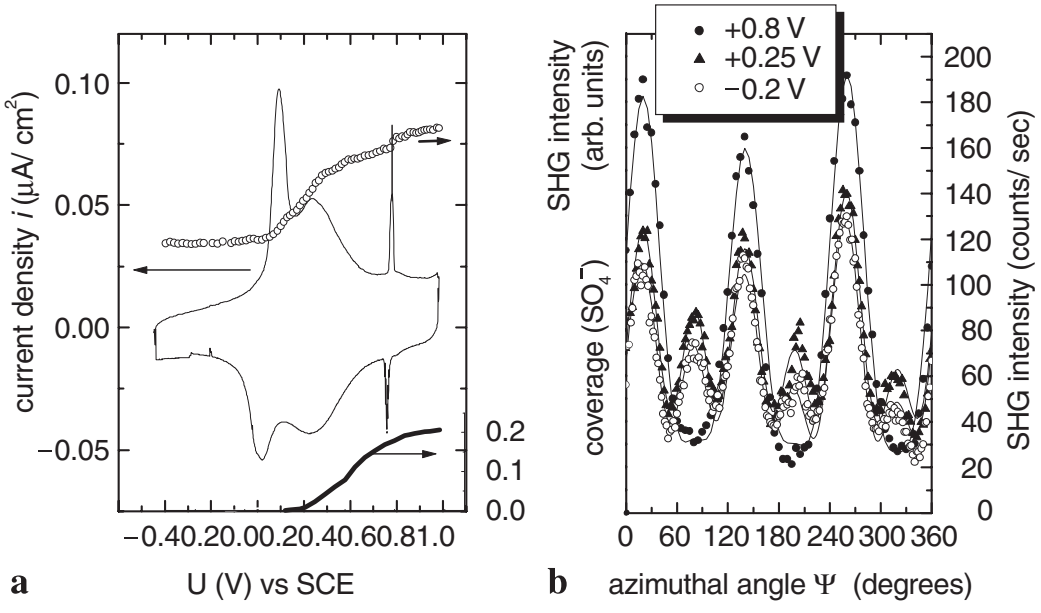

FIGURE 3 Order–disorder surface PT at Au (111) in sulfuric acid: **a** *thin line* – cyclic voltammogram for Au (111) in 0.1 M H_2SO_4 (*left-hand scale*); *thick line* – coverage of (bi)sulfate anions (*right-bottom scale*), the data are taken from [35]; *dots* – SHG intensity at maximum of rotational anisotropy; **b** azimuthal rotational dependences of SHG intensity for *p*-in, *p*-out. Fundamental wavelength is 800 nm

of $\Delta c_3 = c_3\left(\sqrt{3}\times\sqrt{7}\right) - c_3(1\times 1)$ (the increase of c_3 for $U > U_0$ over its value for $U < U_0$, which was averaged over 30 experimental points in the voltage range 0.6–0.78 V) is plotted in Fig. 4a on a logarithmic scale.

The same measurements and calculations have been done for the *s*-in, *s*-out polarisation combination. The three-fold component in this polarisation combination does not show any feature at U_0 (similar to *p*-in, *p*-out). Although for *s*-in, *s*-out an isotropic contribution is forbidden, Fourier analysis shows that $f_0^{ss} \neq 0$. Keeping in mind that for this polarisation combination the one-fold component falls within the error bar, we attributed the observed dependence to the presence of atomic scale inhomogeneities. f_0 increases with increasing voltage and depends linearly on the sulfate-ion coverage (Fig. 4b). No scattered background was found for this system for all measured polarisation combinations.

The absence of hysteresis in the $I_{2\omega}(\Psi)$ dependence, the discontinuity of the derivative (but continuity of the c_3-component itself), and the presence of atomic scale inhomogeneities (rather than islands) all point to the presence at U_0 of a second-order order–disorder PT. This yields, following (10) and (13), a power-law dependence of Δc_3 on the voltage. A linear fit of the experimental dependence $\Delta c_3(U)$ plotted on a logarithmic scale in Fig. 5a gives for the slope 0.22 ± 0.04. The unit cell of $(\sqrt{3}\times\sqrt{7})$ structure is centrosymmetric (see Fig. 5a, inset). Therefore the nonlinear susceptibility in this phase is described by (13) with a quadratic dependence on the order parameter. This means that the critical exponent for this transition is $\beta = 0.11 \pm 0.04$. This value is in agreement with the critical exponent calculated within the framwork of the three-state Potts model with occupied bridge sites ($\beta = 1/12$). Recently, Koper and Lukkien [36] demonstrated using Monte Carlo simulations that the narrow spikes in the CV should be attributed to a second-order PT. The same calculations made for the surface PT studied in our experiment would be very helpful in understanding the nature of the observed PT.

So, in summary, the SHG study of the sulfate-induced disordering of the $(\sqrt{3}\times\sqrt{7})$ structure of an Au (111) surface yielded the following results:

- the SHG field obeys a power-law dependence with critical exponent $\beta = 0.11$, giving the first experimental evidence that it is a second-order PT;
- only atomic scale (and no mesoscopic) inhomogeneities appear to be present on this surface.

4.2.2 First-order order–disorder incommensurate PT in adsorbed layer of sulfamate anions.

An order–disorder PT takes place at an Au (111) surface in the presence of sulfamate anions. Sulfamate anions differ form sulfate anions by replacing one oxygen by an amino group. The CV for Au (111) in sulfamate acid (Fig. 5a) reveals very narrow reversible spikes at U_0=0.2 V. In STM images above 0.2 V, a well-ordered molecular structure is observed [37] and attributed to the sulfamate layer. The unit cell of this structure is almost square (3.81×3.94 Å^2). This structure is incommensurate with respect to the underlying Au (111) as no coincidence lattice was found on a larger scale. The ordered areas form antiphase domains. As no atomic resolution was obtained below U_0, the observed PT was attributed to a structural order–disorder PT [37].

SHG azimuthal dependences in the *p*-in, *p*-out geometry show three maxima for all electrode potentials. Fourier analysis of the azimuthal dependence (using (4)) shows the presence of a one-fold component, but its change with potential falls within the error bar (5%). These observations are consistent with the theoretical analysis for a commensurate–incommensurate phase transition given in Sect. 2.1.2 and allow us to restrict ourselves to measuring the potential dependence of the SHG intensity in the maximum, minimum, and an intermediate point of the azimuthal dependence of the SHG intensity. CVs were measured simultaneously with the SHG scans. The isotropic and anisotropic Fourier components for the *p*-in, *p*-out polarisation combination obtained from these measurements are shown in Fig. 5. The anisotropic three-fold component changes sharply near U_0 (Fig. 5c). The whole change takes place in a wider voltage range than the width of the current spikes and shows a strong hysteresis, in contrast to the CV measurements. It is remarkable to note that the hysteresis exists only for the anisotropic component and not for the isotropic component (Fig. 5b), which is a measure of the surface charge. From the results for c_3 we can calculate using (14) the fraction $H(U)$ of the ordered phase, the results of which are plotted in Fig. 5d.

The dynamics of the surface PT was studied by a modified step-voltage technique. The temporal dependence of applied voltage is shown in Fig. 6a. The current (Fig. 6a) and SHG (Fig. 6b) transients were measured simultaneously. The best

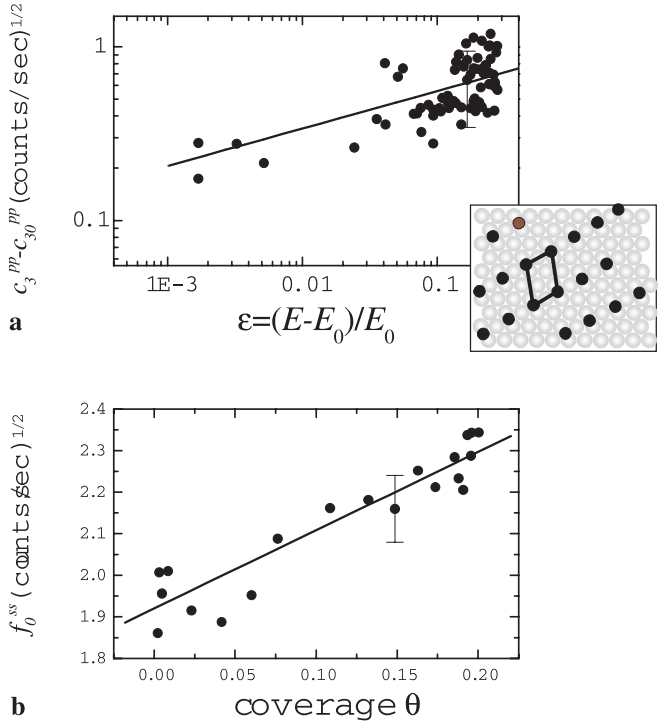

FIGURE 4 Order–disorder surface PT at Au (111) in sulfuric acid: **a** dependence of PT-induced three-fold component Δc_3^{pp} for *p*–*p* polarisation combination on reduced electric field (logarithmic scale); *inset*: the model $(\sqrt{3}\times\sqrt{7})$ structure formed by sulfuric anions; **b** coverage dependence of the forbidden isotropic component in *s*–*s* polarisation combination. Fundamental wavelength is 800 nm

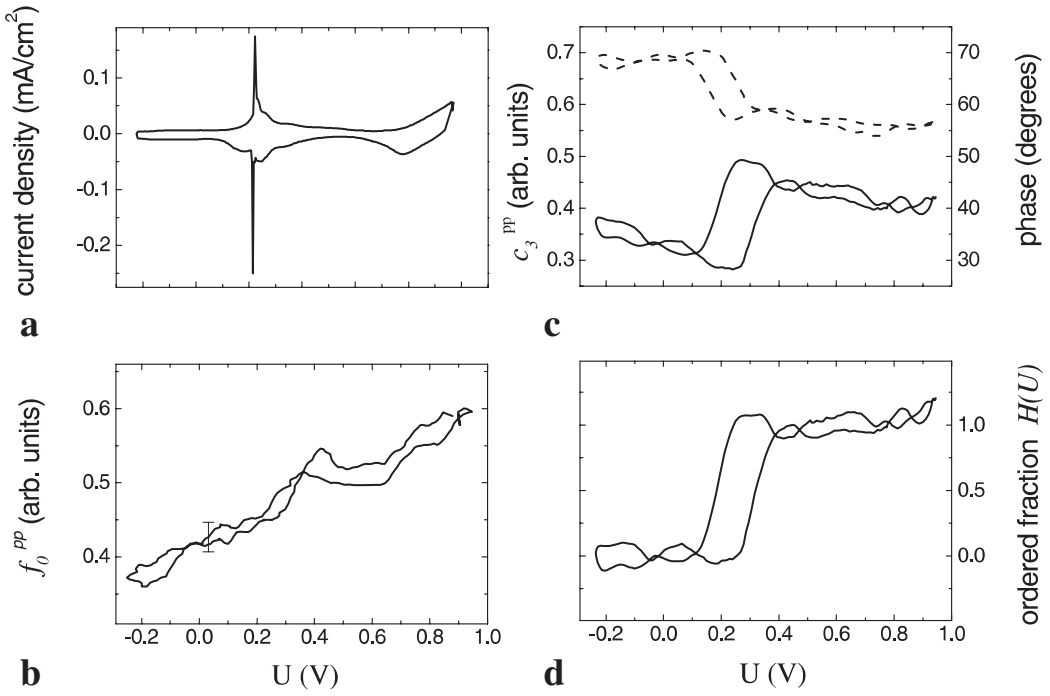

FIGURE 5 Incommensurate surface PT at Au(111) in sulfamate acid: **a** cyclic voltammogram; **b** isotropic component f_0^{pp}; **c** amplitude (*left-hand scale*) and phase (*right-hand scale*) of three-fold component c_3^{pp}; **d** the fraction of the ordered phase. Polarisation combination is *p*-in, *p*-out. Fundamental wavelength is 1064 nm

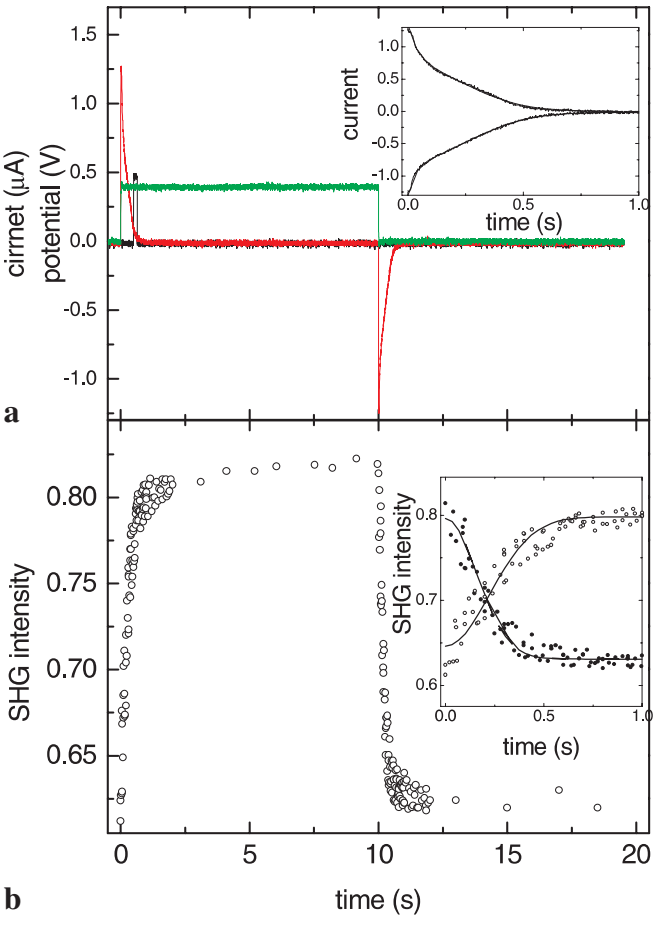

FIGURE 6 Dynamics of incommensurate surface PT at Au(111) in sulfamate acid: **a** step voltage through the surface PT ($0 \leftrightarrow 0.4$ V) and corresponding current transient; *inset*: detailed plot of current transient and fitting by (11) (note that fits can hardly be distinguished from data); **b** SHG transient; *inset*: detailed plot of SHG transient and fitting by (16) (first-order PT model). Fundamental wavelength is 1064 nm

fit was obtained using (11) and (16) for current and SHG transients respectively (nucleation and growth process). This is indicative of the presence of a first-order phase transition. Both for SHG and current the obtained time constant is $t_0 = 0.30 \pm 0.05$ ms.

In summary, for the commensurate–incommensurate phase transition induced by adsorption of sulfamate anions, we find:

- a hysteresis in the anisotropic SHG contribution from which the ordered phase fraction is calculated;
- SHG transients follow a nucleation and growth model, confirming the first-order character of the phase transition.

4.3 *PT in the deposited layer*

We consider here a PT taking place in the epitaxially adsorbed layer of a different metal (so-called underpotential deposition or UPD). Underpotential deposition takes place in an electrochemical environment for potentials close to zero charge and lower than the Nernst potential that determines the beginning of the bulk deposition process (so-called overpotential deposition).

The UPD of copper onto gold(111) electrodes in the presence of sulfate is widely studied experimentally, using electrochemical techniques [38], STM [39], LEED [40], XRD [41], and theoretically [42]. These studies show that two types of transitions occur during the potential scan: with decreasing voltage a disordered structure is formed by Cu adatoms transforming into a co-adsorbed ordered $2(\sqrt{3} \times \sqrt{3})$ or a honeycomb structure with Cu coverage of 2/3 and SO_4 coverage of 1/3. This phase transition PT1 takes place at 0.22 V. With a further decrease of voltage the second phase transition PT2 takes place at 0.07 V, in which sulfate anions are replaced by Cu ions and a Cu (1×1) structure is formed.

The voltammogram of this process is shown in Fig. 7a by a thin line. Peak A (A′) corresponds to PT1, peak B (B′) to PT2. The SHG azimuthal dependence reveals a three-fold symmetry for all phases and no additional Fourier components appeared during these phase transitions. Therefore we measured the SHG intensity (simultaneously with the CV) dependences on the electrode voltage in the minimum, maximum, and intermediate points ($\Psi = 30°$) of the rotational anisotropy. These are shown for the *p*-in, *p*-out polarisation combination in Fig. 7a by thick lines. The changes in SHG intensity are observed at the same positions where current peaks are observed. A strong hysteresis is found for PT2 and no hysteresis was observed (within the error bar) for PT1. The same measurements have been done for the *s*-in, *s*-out polarisation combination. The calculated isotropic and anisotropic Fourier components are presented in Fig. 8(a, b, c).

For the interpretation of these results the voltage dependence of the surface coverage and charge is shown in Fig. 7b, c (plotted with the use of results of [44]).

For the *p*-in, *p*-out polarisation combination the voltage dependence of the isotropic component almost follows the dependence of the total charge (see Fig. 8a, c). Keeping in mind that the charge is modelled and not measured simultaneously, this points in favour of the Dzhavakhidze et al. model [27]. It also means that even for the UPD layer there is no direct contribution to the SHG polarisation from Cu adatoms. The voltage dependence of the amplitude of the three-fold component c_3 in the UPD region is very similar for the *p*-in, *p*-out and the *s*-in, *s*-out. Quantitatively, these dependences are similar to the voltage dependence of sulfate-ion coverage (or partial negative charge). Although it not clear why the anisotropic component is selectively sensitive for negative-ion adsorption, it seems that it can be used as a measure of the surface transformation connected with the anion coverage. The same behaviour was observed for pure sulfuric acid (see Sect. 4.2.1). However, a microscopic analysis of the anisotropic SHG Fourier component is required for a better understanding of these observed dependences.

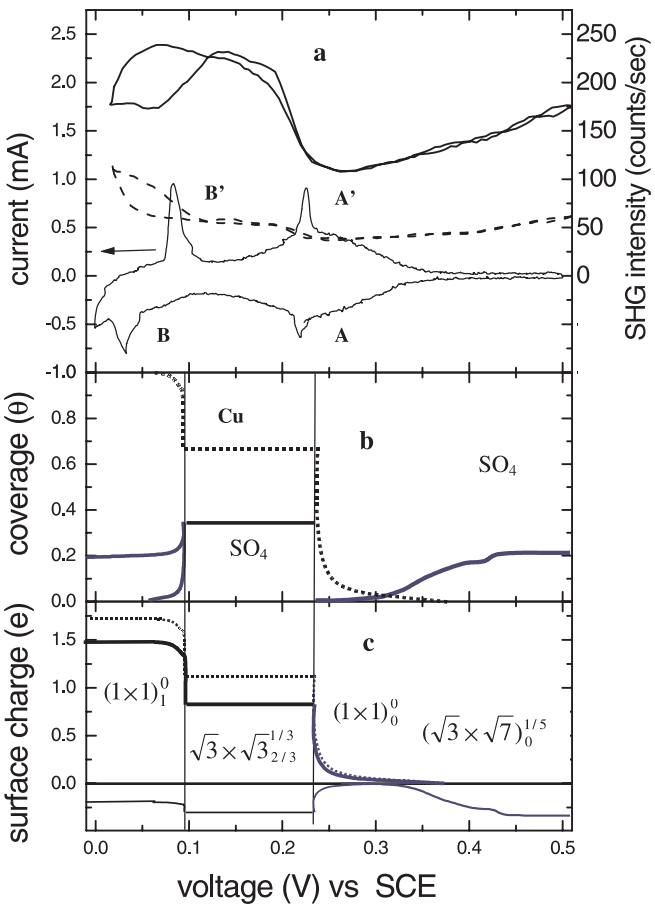

FIGURE 7 Order–disorder and reconstructive PT at Au (111) during underpotential deposition of Cu: **a** cyclic voltammogram (*thin line*, *left-hand scale*) and SHG intensity at maximum (*thick solid line*) and minimum (*dashed line*) of rotational anisotropy; **b** partial coverage of Cu adatoms (*dashed line*) and sulfate anions (*solid line*): data are taken from [44]; **c** surface charge: partials for copper (*dashed line*) and sulfate anions (*thin solid line*) and total (*thick solid line*). Fundamental wavelength is 800 nm

The anodic part of the voltage dependence of the forbidden isotropic component in the *s*-in, *s*-out polarisation combination is similar to the case of pure sulfuric acid: for both a smooth increase is observed while the concentration of randomly adsorbed sulfate anions increases. In the UPD region (PT1) a peak in f_0(U) is observed. This behaviour confirms the presence of randomly adsorbed species on an atomic scale. In this process a voltage dependence of scattered radiation was observed (see Fig. 8d) as well. The minimum of this dependence corresponds to the pure 1×1 Au substrate. An increase of the scattered radiation is observed in the UPD region and anodic regions that points to a formation of inhomogeneities on a mesoscopic scale.

In order to find the order of these transitions, time-resolved measurements have been performed. The SHG intensity has been measured at the maximum of the rotational anisotropy. Simultaneously the current transients were measured. The left-hand panel in Fig. 9 shows the temporal dependence of the SHG intensity and the corresponding current transient during a periodic voltage step $0.15 \rightarrow 0.5$ V (that overlaps peak A (A′) in CV). Both SHG and current transients were fitted using models of random nucleation and nucleation and growth. The best fit was obtained using a nucleation and growth model both for the current and SHG transients. However, the time constants of the SHG process are at least five times larger than for the current transient. As the SHG signal at the maximum contains information about both isotropic and anisotropic components, and the latter reveals the symmetry properties, slower processes that do not influence the current but influence the ordering at the surface (like diffusion) may slow down the SHG response. The right-hand panel in Fig. 9 shows the SHG and current transients during a periodic voltage step $0 \rightarrow 0.15$ V (that overlaps peak B in the CV). No change of SHG intensity is observed during this step. The current transients do not fall to zero within the present time range. It means that the time constant of PT2 is given by $t_{PT2} \gg 50$ ms, which is consistent with the results of [42, 43].

In summary, for the underpotential deposition of Cu on Au (111) in the electrochemical cell, in the presence of sulfate ions we find:

– the SHG transients are consistent with a nucleation and growth model, confirming the first-order character of this order–disorder phase transition;

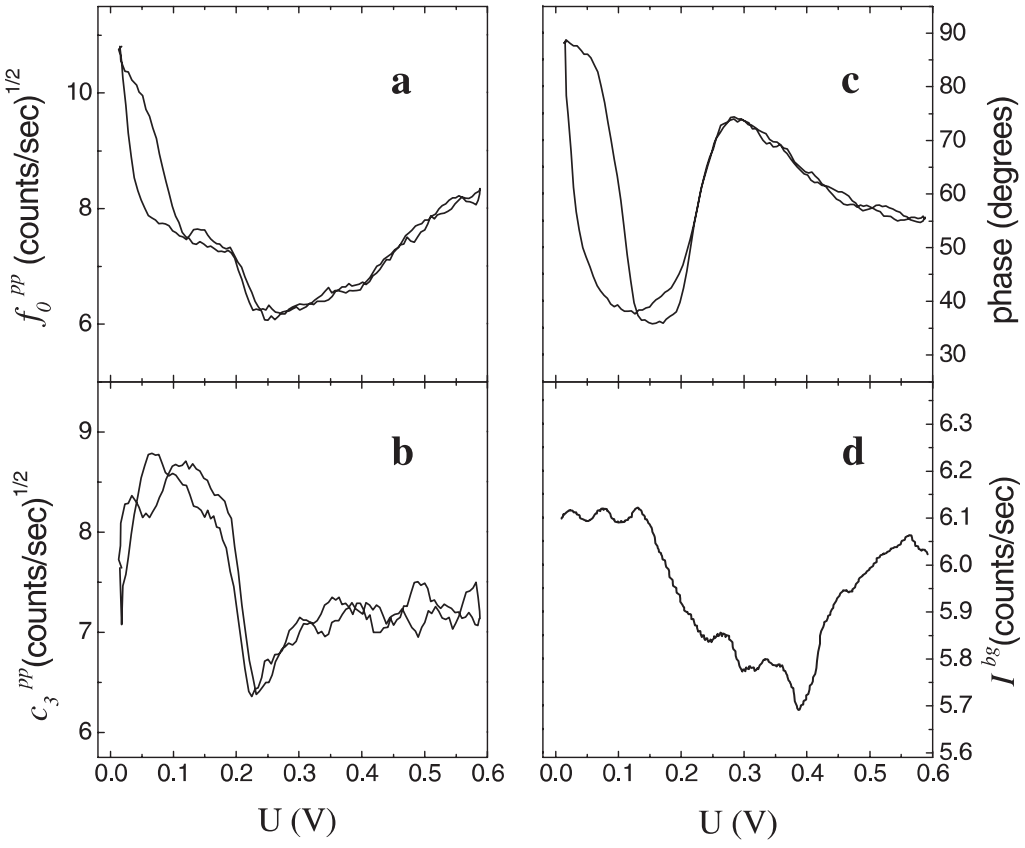

FIGURE 8 Order–disorder and reconstructive PT at Au(111) during underpotential deposition of Cu for p–p polarisation combination: isotropic component f_0^{pp} **a**; amplitude and phase of three-fold component c_3^{pp} **b, c**; scattered SHG intensity at the scattering angle of 20° **d**. Fundamental wavelength is 800 nm

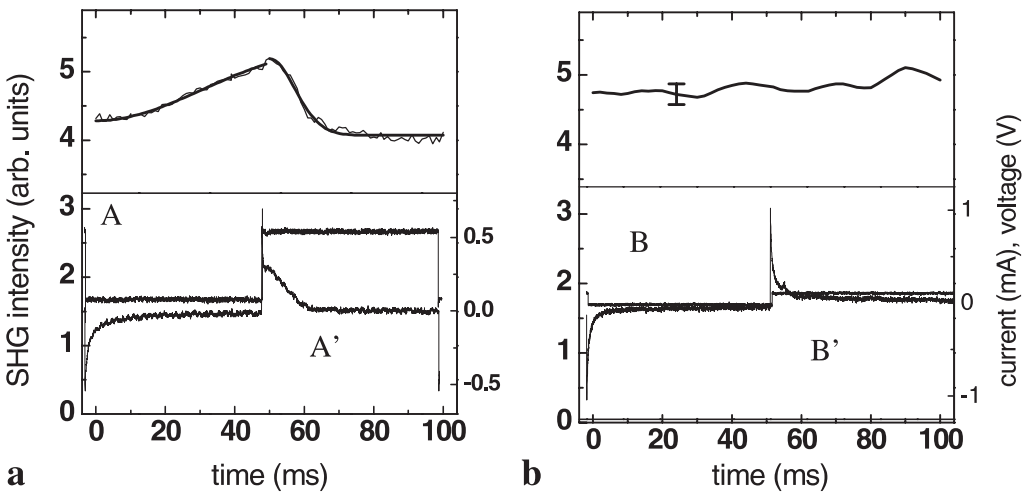

FIGURE 9 Dynamics of order–disorder and reconstructive PT at Au(111) during underpotential deposition of Cu: step voltage, current transient (*right-hand scale*, *bottom*) and SHG transient (*left-hand scale*) for PT1 **a** and PT2 **b**. *Capital letters* indicate corresponding current peaks of CV (see Fig. 7a). Fundamental wavelength is 1064 nm

– SHG scattered radiation is observed during the PT, which indicates mesoscopic scale inhomogeneities (nuclei formation) in the vicinity of the phase transition;
– atomic scale inhomogeneities increase in the vicinity of the order–disorder phase transition.

5 Conclusions

We have developed a general approach for the study of (near-)surface phase transitions by SHG techniques. This approach implies (i) a theoretical and experimental analysis of the SHG azimuthal dependences of the specular and scattered components, (ii) a deconvolution from the experimental results of the dependences of the SHG field on the PT-inducing external parameters, and (iii) analysing the obtained dependences in relation to the thermodynamic classification of phase transitions. For a second-order PT we developed a phenomenological model correlating the order parameter with the SHG field.

The suggested approach is applied to the studies of different types of (near-)surface PTs for which the advantages of the SHG technique were clearly demonstrated. In particular, we studied PTs at buried (solid/solid and solid/liquid) interfaces, i.e. the systems that are hardly accessible by most commonly used techniques. The dynamics of some of the phase transitions studied enabled the additional separation between first- and second-order PTs.

ACKNOWLEDGEMENTS This work was partly supported by the Research for the Future (RFTF) program by the Japan Society for the Promotion of Science, by the Nederlandse Organisatie voor Wetenschappelijk Onderzoek (Grant No. NWO 1604-1999), and by the Russian Foundation of Basic Research (Grant No. 00-02-16 557). The authors thank Prof. J. Lipkowski and Dr. A.V. Petukhov for useful discussions.

REFERENCES

1 C.V. Shank, R. Yen, S. Hirlimann: Phys. Rev. Lett. **51**, 900 (1983)
2 T.F. Heinz, M.M.T. Loy, W.A. Thompson: Phys. Rev. Lett. **54**, 63 (1985)
3 D.M. Kolb: Electrochem. Acta **45**, 2387 (2000)
4 E. Bauer: in *Structure and Dynamics of Surfaces II*, ed. by W. Schommers, P. Von Blanckenhagen (Springer, Berlin 1985) pp. 115–179
5 V.H. Etgens, M.C. Martins Alves, A. Tadjeddine: Electrochim. Acta **45**, 591 (1999)
6 G. Lupke: Surf. Sci. Rep. **35**, 75 (1999)
7 J.A. Litwin, J.E. Sipe, H.M. Van Driel: Phys. Rev. B **31**, 55 (1985)
8 A. Rudnick, E.A. Stern: Phys. Rev. B **4**, 4274 (1971)
9 O.A. Aktsipetrov, A.V. Melnikov, T.V. Murzina, A.A. Nikulin, A.N. Rubtsov: Surf. Sci. **336**, 225 (1995)
10 B. Pettinger, J. Lipkowski, S. Mirwald: Electrochim. Acta **40**, 133 (1995)
11 J.I. Dadap, B. Doris, Q. Deng, M.C. Downer, J.K. Lowell, A.C. Diebold: Appl. Phys. Lett. **64**, 2139 (1994)
12 S.T. Cundiff, W.H. Knox, F.H. Baumann, K.W. Evans-Lutterodt, M.-T. Tang, L. Green, H.M. van Driel: Appl. Phys. Lett. **70**, 1414 (1997)
13 E.D. Mishina, A.A. Fedyanin, D.A. Klimkin, A.A. Nikulin, O.A. Aktsipetrov, S.L. Vorob'eva, V.R. Novak, M.A.C. Devillers, T. Rasing: Surf. Sci. **382**, L696 (1997)
14 O.A. Aktsipetrov, A.A. Fedyanin, D.A. Klimkin, A.A. Nikulin, E.D. Mishina, A.S. Sigov, K.A. Vorotilov, M.A.C. Devillers, T. Rasing: Ferroelectrics **190**, 143 (1997)
15 W. Daum, H.-J. Krause, U. Reichel, H. Ibach: Phys. Rev. Lett. **71**, 1234 (1993)
16 V.I. Gavrilenko, R.Q. Wu, M.C. Downer, J.G. Ekkerdt, D. Lim, P. Parkinson: Thin Solid Films **364**, 1 (2000)
17 B.S. Mendoza, A. Gaggiotti, R. Del Sole: Phys. Rev. Lett. **81**, 3781 (1998)
18 C.M. Li, L.E. Urbach, H.L. Dai: Phys. Rev. B **49**, 2104 (1994)
19 A.V. Petukhov: Surf. Sci. **347**, 143 (1996)
20 L.J. Simpson, T.E. Furtak: J. Electroanal. Chem. **500**, 163 (2001)
21 S. Reiff, J.H. Block: Surf. Sci. **345**, 281 (1996)
22 E.D. Mishina, T.V. Misuryaev, N.E. Sherstyuk, V.V. Lemanov, A.I. Morozov, A.S. Sigov, T. Rasing: Phys. Rev. Lett. **85**, 3664 (2000)
23 B.N.J. Persson: Surf. Sci. Rep. **15**, 1 (1992)
24 A. Bewick, M. Flieshman, H.R. Tsirsk: Trans. Faraday Soc. **58**, 2200 (1962)
25 F.E. Varela, L.M. Grassa, J.R. Vilche: Electrochim. Acta **37**, 1119 (1992)
26 V.L. Ginzburg, A.P. Levanyuk, A.A. Sobyanin: Phys. Rep. **57**, 151 (1980)
27 P.G. Dzhavakhidze, A.A. Kornyshev, A. Liebsch, M. Urbakh: Phys. Rev. B **45**, 9339 (1992)
28 E. Mishina, N. Ohta, Q.-K. Yu, S. Nakabayashi: Surf. Sci. **494**, L748 (2001)
29 S. Mirlad, B. Pettinger, J. Lipkowski: Surf. Sci. **335**, 264 (1995)
30 E.D. Mishina, N.E. Sherstyuk, A.I. Morozov, A.S. Sigov, O.A. Aktsipetrov, V.V. Lemanov, T. Rasing: JETP **94**, 552 (2002)
31 E. Mishina, Q.-K. Yu, S. Nakabayashi: in preparation
32 M. Giesen, D.M. Kolb: Surf. Sci. **468**, 149 (2000)
33 M.S. Zei, D.A. Scherson, G. Lehmpfunh, D.M. Kolb: J. Electroanal. Chem. **229**, 99 (1987)
34 O.M. Magnussen, J. Hageböck, J. Hotlos, R.J. Behm: Faraday Discuss. **94**, 329 (1992)
35 Z. Shi, J. Lipkowski, M. Camboa, P. Zelenay, A. Wieckowski: J. Electroanal. Chem. **366**, 317 (1994)
36 M.T.M. Koper, J.J. Lukkien: J. Electroanal. Chem. **485**, 161 (2000)
37 J.L. Bubendroff, L. Cagnon, V. Costa-Kieling, J.P. Bucher, P. Allongue: Surf. Sci. **384**, L836 (1997)
38 J.W. Schultze, D. Dikkertmann: Surf. Sci. **54**, 489 (1976)
39 T. Hachiya, H. Honbo, K. Itaya: J. Electroanal. Chem. **315**, 275 (1991)
40 J. Zhang, Y.-E. Sung, P.A. Rikvold, A. Wieckowski: J. Chem. Phys. **104**, 5699 (1996)
41 M.F. Toney, J.N. Howard, J. Richer, G.L. Borges, J.G. Gordon, O.R. Merloy, D. Yee, L.B. Sorensen: Phys. Rev. Lett. **75**, 4472 (1995)
42 P.A. Rickvold, G. Brown, N.A. Novotny, A. Wieckowski: Colloids Surf. A **134**, 3 (1998)
43 P.A. Rikvold, A. Wieckowski: in *Thin Films and Phase Transitions on Surfaces*, ed. by M. Michailov (Institute of Physical Chemistry Bulgarian Academy of Sciences, Sofia 1996)
44 Z. Shi, J. Lipkowski: J. Electroanal. Chem. **364**, 289 (1994)